Tissue-specific reduction in MLH1 expression induces microsatellite instability in intestine of Mlh1+/- mice

Shrestha, Kul

2021-10

Shrestha , K , Aska , E , Tuominen , M & Kauppi , L 2021 , ' Tissue-specific reduction in MLH1 expression induces microsatellite instability in intestine of Mlh1+/- mice ' , DNA Repair , vol. 106 , 103178 . https://doi.org/10.1016/j.dnarep.2021.103178

http://hdl.handle.net/10138/333506
https://doi.org/10.1016/j.dnarep.2021.103178

DNA Repair 106 (2021) 103178

Contents lists available at ScienceDirect

DNA Repair

journal homepage: www.elsevier.com/locate/dnarepair

Tissue-specific reduction in MLH1 expression induces microsatellite instability in intestine of *Mlh1*$^{+/-}$ mice

Kul S. Shrestha [a,b,c], Elli-Mari Aska [a,b,c], Minna M. Tuominen [a,1], Liisa Kauppi [a,c,*]

[a] Systems Oncology (ONCOSYS) Research Program, Research Programs Unit, Faculty of Medicine, University of Helsinki, Helsinki, Finland
[b] Doctoral Program in Integrative Life Sciences, University of Helsinki, Helsinki, Finland
[c] Department of Biochemistry and Developmental Biology, Faculty of Medicine, University of Helsinki, Helsinki, Finland

ARTICLE INFO

Keywords:
Lynch syndrome
Mlh1 haploinsufficiency
Microsatellite instability
Mlh1 promoter methylation

ABSTRACT

Tumors of Lynch syndrome (LS) patients display high levels of microsatellite instability (MSI), which results from complete loss of DNA mismatch repair (MMR), in line with Knudson's two-hit hypothesis. Why some organs, in particular those of the gastrointestinal (GI) tract, are prone to tumorigenesis in LS remains unknown. We hypothesized that MMR is haploinsufficient in certain tissues, compromising microsatellite stability in a tissue-specific manner before tumorigenesis. Using mouse genetics, we tested how levels of MLH1, a central MMR protein, affect age- and tissue-specific microsatellite stability *in vivo* and whether elevated MSI is detectable prior to loss of MMR function and to neoplastic growth.

To assess putative tissue-specific MMR haploinsufficiency, we determined relevant molecular phenotypes (MSI, *Mlh1* promoter methylation status, MLH1 protein and RNA levels) in jejuna of *Mlh1*$^{+/-}$ mice and compared them to those in spleen, as well as to MMR-proficient and -deficient controls (*Mlh1*$^{+/+}$ and *Mlh1*$^{-/-}$ mice). While spleen MLH1 levels of *Mlh1*$^{+/-}$ mice were, as expected, approximately 50 % compared to wildtype mice, MLH1 levels in jejunum varied substantially between individual *Mlh1*$^{+/-}$ mice and moreover, decreased with age. *Mlh1*$^{+/-}$ mice with soma-wide *Mlh1* promoter methylation often displayed severe MLH1 depletion in jejunum. Reduced (but still detectable) MLH1 levels correlated with elevated MSI in *Mlh1*$^{+/-}$ jejunum. MSI in jejunum increased with age, while in spleens of the same mice, MLH1 levels and microsatellites remained stable. Thus, MLH1 expression levels are particularly labile in intestine of *Mlh1*$^{+/-}$ mice, giving rise to tissue-specific MSI long before neoplasia. A similar mechanism likely also operates also in the human GI epithelium and could explain the wide range in age-of-onset of LS-associated tumorigenesis.

1. Introduction

Lynch syndrome (LS) is an autosomal-dominant cancer syndrome characterized by a high risk of developing colorectal cancer (CRC), endometrial cancer and various other cancers. LS accounts for 1–5 % of all CRC cases; individuals with LS have >80 % lifetime risk of developing CRC and are diagnosed with CRC at an average age of 44 years. LS patients carry germline heterozygous mutations in one of the DNA mismatch repair (MMR) genes, typically *MLH1* and *MSH2* [1–3]. MMR is required for the repair of single base pair mismatches and small insertion-deletion (indel) mutations which arise from strand-slippages during DNA replication [4,5]. Microsatellites (short DNA tandem repeats), because of their repetitive nature, are highly prone to such replication errors [4,6], which if left unrepaired leads to indel mutations in MMR-deficient cells, a phenotype known as microsatellite instability (MSI) [4,7]. High-level MSI is a molecular hallmark of LS patients' tumors and indicates defective MMR [8,9]. The conventional notion of MSI in LS-associated CRC is that it follows Knudson's two-hit hypothesis [10]: both MMR alleles must be defective in order to trigger MSI. In this model, the first hit is inherited as a germline defect in an MMR gene, and the remaining functional MMR allele is lost (i.e. second hit) by somatic mutations, epigenetic inactivation or loss of heterozygosity (LOH),

* Corresponding author at: Systems Oncology (ONCOSYS) Research Program, Research Programs Unit, Faculty of Medicine, University of Helsinki, Helsinki, Finland.
E-mail address: Liisa.Kauppi@helsinki.fi (L. Kauppi).
[1] present address: FIMM Sequencing Unit, FIMM Technology Centre, Finnish Institute for Molecular Medicine (FIMM), Helsinki Institute of Life Science (HiLife), University of Helsinki, Helsinki, Finland.

https://doi.org/10.1016/j.dnarep.2021.103178
Received 11 May 2021; Received in revised form 6 July 2021; Accepted 7 July 2021
Available online 9 July 2021

leading to a complete loss of MMR function (MMR deficiency) that initiates the MSI mutator phenotype, subsequently instigating tumorigenesis [11–13].

Certain observations, however, suggest that MMR genes may be haploinsufficient, i.e., that loss of function of just one allele may lead to compromised genome integrity. Firstly, LS patients show low-level MSI in peripheral blood leukocytes and in normal colon mucosa [14–16]. Additionally, cell-free extracts from *Mlh1*$^{+/-}$ mouse embryonic fibroblasts show decreased MMR activity [7], low MMR levels reduce MMR efficiency in non-neoplastic human cell lines [17,18], and *Mlh1* hemizygosity increases indel mutations in cancer cell lines [19]. Given these hints of MMR haploinsufficiency, we hypothesized that reduced MMR protein levels may provoke microsatellite instability in certain tissues, such as the highly proliferating (and tumor-prone) intestinal epithelium in mice, already prior to the "second hit".

The MSI mutator phenotype and MMR deficiency associated tumor spectrum has been extensively characterized in a constitutional *Mlh1* knock-out mouse model (*Mlh1*$^{-/-}$ mice), and these animals have a high incidence of MMR-deficient MSI-high GI tumors [7,20–22]. Unlike in humans, GI tumorigenesis in MMR-deficient mice preferentially affects the small intestine (in particular, jejunum and ileum) and not the colon [20], thus in MMR mouse models, small intestine is used to study the cellular and molecular phenotypes related to GI tumorigenesis [21, 23–25]. Here, we used *Mlh1* heterozygous (*Mlh1*$^{+/-}$) mice [7,22] as model of LS to test tissue-specific MMR haploinsufficiency. As in LS, *Mlh1*$^{+/-}$ mice have early-onset of GI tract tumors, and increased mortality [21].

To test the effect of age and *Mlh1* heterozygosity on MSI in jejunum, we used sensitive single-molecule PCR to quantify MSI in normal jejunum of 4- and 12-month-old *Mlh1*$^{+/-}$ mice, and compared MSI rates with those from jejunum of age-matched *Mlh1*$^{+/+}$ mice. To study the tissue-specificity of MSI, we compared the jejunum MSI data with (recently published [26] and additional) spleen MSI data from the same mice. In addition, we assayed MSI in *Mlh1*$^{-/-}$ jejuna at both time points, and in an intestinal tumor from a 12-month-old *Mlh1*$^{-/-}$ mouse. We also measured Mlh1 mRNA and MLH1 protein expression levels in different organs of *Mlh1*$^{+/-}$ mice, focusing on the comparison between the small intestine (highly proliferative [27] and tumor-prone) and spleen (less proliferating [28] and no MMR-dependent tumors reported) to assess the correlation of MLH1 expression with MSI. Finally, we tested loss of heterozygosity (LOH) and promoter methylation at *Mlh1* as possible explanations for the tissue-specific reduction in MLH1 expression.

2. Methods

2.1. Mice and genotyping

Mlh1 mice (B6.129- *Mlh1*^{tm1Rak}, strain 01XA2, National Institutes of Health, Mouse Repository, NCI-Frederick) [7] were bred and maintained according to national and institutional guidelines (Animal Experiment Board in Finland and Laboratory Animal Centre of the University of Helsinki). *Mlh1* genotyping was performed using ear pieces as previously described [26]. In total, 57 mice (38 males and 19 females) were used in this study. DNA, RNA and protein (western blot) analyses were performed in same set of mice (see **Supplementary Table 2**). For this, a total of 35 mice were used, and the numbers of *Mlh1*$^{+/+}$, *Mlh1*$^{+/-}$ and *Mlh1*$^{-/-}$ mice were: 5, 12 and 3 at 4-month and 3, 10 and 2 at 12-month time points, respectively. In addition, ten 1-month-old mice were used for RNA analysis: 3 *Mlh1*$^{+/+}$, 5 *Mlh1*$^{+/-}$ and 2 *Mlh1*$^{-/-}$ mice. A different set of twelve mice, all 4 months old, were used for immunohistochemistry (IHC), as follows: 4 *Mlh1*$^{+/+}$, 6 *Mlh1*$^{+/-}$ and 2 *Mlh1*$^{-/-}$ mice. The number of mice for each experiment, along with genotype and age, is indicated in the respective figures in the results section. A subset of mice (18 male mice: 3 *Mlh1*$^{+/+}$ and 6 *Mlh1*$^{+/-}$ mice each for 4- and 12-month time point) used in this study were the same mice for which MSI and methylation status of *Mlh1* promoter in sperm and spleen was assayed in our recent publication [26].

2.2. Tissue collection for DNA, RNA and protein analysis

The small intestine was flushed with cold phosphate-buffered saline (PBS), cut open longitudinally and visually inspected for visible tumors. A 3cm long piece of jejunum was cut approximately 15 cm from the pyloric sphincter. This tissue piece, henceforth referred to simply as "jejunum", was approximately the center of the small intestine. Jejunum was inspected for any macroscopic tumor-like outgrowth under a stereoscope, and only normal-looking tissue pieces were used for the experiments. The jejunum was snap-frozen and stored at −80 °C. Other tissues and *Mlh1*$^{-/-}$ intestinal tumors were also collected, snap-frozen and stored at −80 °C. Frozen tissues were used for subsequent DNA, RNA and protein analysis.

2.3. DNA extraction and single-molecule MSI analysis by PCR

MSI was assayed at the single-DNA molecule level, as described previously [26]. Briefly, DNA was extracted using AllPrep DNA/RNA/Protein Mini Kit (Qiagen, Hilden, Germany) according to manufacturer's instructions. Approximately 5 mg of tissue was used for DNA extraction. The extracted DNA was quantified using a Qubit fluorometer (Thermo Fisher Scientific, Waltham, MA) and diluted to 30 pg/µl concentration in 5 mM Tris-HCl (pH 7.5) supplemented with 5 ng/µl carrier herring sperm (Thermo Fisher Scientific). The MSI assay was performed using single-molecule PCR (SM-PCR) [26,29]. Three microsatellites, two mononucleotide repeats A27 and A33 [30], and a dinucleotide repeat D14Mit15 [7] were assayed for MSI. To ensure that individual PCRs are seeded with a single amplifiable DNA molecule, we estimated the number of amplifiable molecules by using a dilution series (30 pg, 6 pg, 4.5 pg and 0.6 pg of input DNA) for each DNA sample analyzed, similar to previous reports [26,31]. We determined the DNA concentration that yielded a PCR product in approximately 50 % of reactions. By Poisson approximation, this PCR success rate equates to approximately one amplifiable molecule per positive reaction [26,29,31,32]. SM-PCR methodology (including PCR primers and cycling conditions) was described in detail previously [26]. DNA fragments were analyzed by capillary electrophoresis, using ABI3730xl DNA Analyzer (Thermo Fisher Scientific). Between 116 and 205 amplifiable DNA molecules per tissue per mouse were assayed for each microsatellite locus. Data was analyzed using Fragman R package [33]. The mutation rates reported here are likely a conservative estimate, because stringent criteria were used for true microsatellite signal calling and for mutant calling, as described previously [26]. In brief, as a true microsatellite signal should have stutter peaks, signals without stutter peaks were considered artifacts. An allele was scored as mutant only when the highest peak and the stutter peaks shifted as one unit; shift of the highest peak only was not considered as mutant allele. In case of co-occurrence of a wild-type allele and a mutant allele in a single PCR, the reaction was scored as wild-type allele. For each microsatellite, MSI was scored separately for insertions and deletions in terms of number of single repeat-unit shifts observed.

MSI rate = total number of single repeat unit shifts observed / total DNA molecules analyzed

Hence, MSI rate equals 1 if every DNA molecule analyzed in the sample has a single repeat unit shift. If some DNA molecules have larger (>single repeat unit) shifts, then MSI rate can be >1.

2.4. RNA extraction and RNA expression analysis

RNA was extracted using AllPrep DNA/RNA/Protein Mini Kit (Qiagen) according to manufacturer's instructions. Extracted RNA was measured using NanoDrop 1000 spectrophotometer (Thermo Fisher Scientific, Waltham, MA). 500 ng of extracted RNA was reverse-

transcribed using SuperScript VILO cDNA Synthesis Kit (Invitrogen). Quantitative PCR (qPCR) was performed in CFX96 Touch Real-Time PCR Detection System (Bio-Rad) using SsoAdvance Universal SYBR Green Supermix system (Bio-Rad, Hercules, CA). PCR conditions were as follows: 30 s at 95 °C, 40 cycles of 10 s at 95 °C, 30 s at 60 °C, and 5 s at 72 °C. The following primers were used for qPCR: for Mlh1, forward primer 5′ GGGAGGACTCTGATGTGGAA 3′ and reverse primer 5′ AGAGCTTGGTCTGGTGCTGT 3′ (amplicon size: 216 bp), and for beta-actin, forward primer 5′ AGACTTCGAGCAGGAGATGG 3′ and reverse primer 5′ AGGTCTTTACGGATGTCAACG 3′ (amplicon size: 210 bp). Gene expression data of Mlh1 was normalized to beta-actin. Data was analyzed using Bio-Rad CFX Maestro (version 1.1).

2.5. Western blot analysis

Frozen tissue pieces were thawed on ice, mechanically homogenized in RIPA buffer supplemented with protease inhibitor cocktail (Roche, Basel, Switzerland), incubated for 30 min on ice and centrifuged at 14,000 rpm for 10 min at 4 °C. The supernatant was collected and stored at −80 °C until further use. Total protein concentration was measured using Pierce™ BCA™ protein assay kit (Thermo Fisher Scientific), 30 μg of total protein extract was used for western blotting. The denatured protein was run in 4–20 % gradient Mini-Protean TGX gels (Bio-Rad) and transferred to 0.2 μm nitrocellulose membrane using Trans-Blot Transfer Pack (Bio-Rad). To confirm complete protein transfer, membranes were stained with Ponceau solution for 5 min at room temperature. Membranes were blocked with 5% milk in PBS supplemented with 1 μl/mL Tween-20 (Thermo Fisher Scientific) for 1 h at room temperature, and incubated overnight at 4 °C with primary antibodies against MLH1 (1:1000, Abcam, Cambridge, UK, catalog no. ab92312), and Beta-actin (1:5000, Sigma, Missouri, USA, catalog no. A5441), followed the next day by infrared IRDye 800CW (1:5000, Li-COR, Nebraska, USA, catalog no. 926-32211) and IRDye 680RD (1:5000, Li-COR, catalog no. 926-68070) secondary antibody incubation for 1 h at room temperature. LI-COR Odyssey FC system (LI-COR) was used to scan the membranes and LI-COR Image Studio lite (version 5.2) was used for image analysis. MLH1 protein signal intensities were normalized to beta-actin signal intensity.

2.6. Immunohistochemistry (IHC) and histological image analysis

The small intestine was flushed with cold 1xPBS, fixed overnight in 4% paraformaldehyde, cut open longitudinally, embedded into paraffin blocks as a “Swiss roll” [34], and sectioned at 4 μm thickness. Heat-induced antigen retrieval was performed for 20 min using 10 mM citrate buffer (pH 6). MLH1 was detected using anti-MLH1 antibody (1:1500, Abcam, catalog no. ab92312), and visualized using Bright-Vision Poly HRP goat anti-rabbit IgG (ImmunoLogic, Duiven, The Netherlands, catalog no. DPVR55HRP). Sections were counterstained with hematoxylin-eosin. Slides were scanned using 3DHistech Panoramic 250 FLASH II digital slide scanner (3DHistech, Budapest, Hungary) at 20X magnification, and images were visualized using CaseViewer (version 2.2). For each mouse, MLH1 protein levels were quantified for five randomly selected sites in the jejunum, each site consisting of approximately ten villus-crypt units, altogether approximately 50 villus-crypt units per jejunum. Quantification was performed using IHC Profiler plugin in ImageJ [35].

2.7. Mlh1 LOH analysis

LOH was tested using restriction fragment length polymorphism (RFLP) assay on two large PCR products that covered approximately 20 % of the *Mlh1* gene in total, and were located at the far 5′ and 3′ ends of the *Mlh1* gene. These regions spanned exons 1 and 19, respectively, and we refer to them as RFLP_exon 1 and RFLP_exon 19 from here on (Fig. 3A). 50 ng of DNA was seeded into each PCR which was performed using Phusion High-Fidelity DNA Polymerase system (Thermo Fisher Scientific). The following primers were used: for RFLP_exon 1, forward primer 5′ GGCTTACCTGCCAGCACAACC 3′ and reverse primer 5′ CCGTGTGCATAATGGGAAACC 3′, and for RFLP_exon 19, forward primer 5′ GAGTATGCCAGTAGCTGGGAG 3′ and reverse primer 5′ CAGTTCAAAGATCGGGCAAG 3′. PCR conditions were as follows: 30 s at 98 °C, 35 cycles of 10 s at 98 °C, 20 s at 70 °C and 120 s at 72 °C, followed by 10 min at 72 °C. PCR product sizes of RFLP_exon 1 and RFLP_exon 19 were 4 kb and 5.7 kb, respectively. 200 ng of PCR product of RFLP_exon1 and RFLP_exon 19 were digested with *Pst*I (New England Biolabs) and *Vsp*I (Thermo Fisher Scientific) restriction enzymes, respectively, according to manufacturer’s instruction. $Mlh1^{+/+}$ and $Mlh1^{-/-}$ jejunum DNA was used as normal and knock-out allele controls, respectively. Digested PCR products were analyzed by gel electrophoresis on an ethidium bromide stained 1.5 % agarose gel. DNA samples were considered to have undergone LOH if the samples displayed the same banding pattern as the PCR seeded with $Mlh1^{-/-}$ DNA.

2.8. Mlh1 promoter methylation analysis by methylation-specific PCR (MSP)

Methylation status of the *Mlh1* promoter was tested by MSP, as described previously [26]. Briefly, 200 ng of genomic DNA was bisulfite-converted, and 2 μl of bisulfite-converted DNA was used for MSP. Two different PCRs were set up in parallel, one with a primer pair specific to methylated CpG sites at the *Mlh1* promoter (forward primer 5′ GGTGTACGAAGTTATTTTTATTTTAGTC 3′ and reverse primer 5′ ACCCAACGATACCTAATAATAAAACC 3′) (Zymo Research, Irvine, CA, catalog no. D2012), and another with a primer pair specific to unmethylated CpG at the same sites (forward primer 5′ GGTGTATGAAGTTATTTTTATTTTAGTT 3′ and reverse primer 5′ ACCCAACAATACCTAATAATAAAACC 3′). PCR conditions were as follows: 10 min at 95 °C, 40 cycles of 30 s at 95 °C, 45 s at 58 °C and 60 s at 72 °C, followed by 7 min at 72 °C. PCRs were performed in triplicate, and run on a 1.5 % agarose gel stained with ethidium bromide and visualized by UV light. A sample was scored as *Mlh1* promoter methylated if all MSP triplicates (with primers specific to methylated CpG sites) displayed a PCR product. Faint PCR products were also scored as *Mlh1* promoter methylated, as long as they were seen across triplicates.

2.9. Statistical analysis

Statistical testing was done using an unpaired *t*-test, and linear regression fitting was tested using F-test. Two-tailed P-values < 0.05 were considered statistically significant.

3. Results

3.1. Normal jejunum of $Mlh1^{+/-}$ mice displays MSI

We investigated the effect of *Mlh1* heterozygosity on *Mlh1* expression levels and on microsatellite stability in the intestine, in both younger and older mice (Fig. 1A). Spleen was used as a control for tissue-specificity. MSI was quantified by highly sensitive SM-PCR on three microsatellite loci (two mononucleotide repeats and one dinucleotide repeat, Fig. 1B) in 4- and 12-month-old $Mlh1^{+/-}$ mice. $Mlh1^{+/+}$ and $Mlh1^{-/-}$ tissues were used as MMR-proficient and MMR-deficient controls, respectively, and MSI was also assessed in an intestinal tumor from a 12-month-old $Mlh1^{-/-}$ mouse.

Compared to age-matched $Mlh1^{+/+}$ jejuna, in $Mlh1^{+/-}$ jejuna deletions at mononucleotide repeats were elevated (observed deletions were predominantly single repeat unit, i.e., 1 bp shifts) (Fig. 1**C**,**D**), while the dinucleotide repeat D14Mt15 was stable (**Supplementary Fig. 1**). At 4 and 12 months, $Mlh1^{+/-}$ jejuna showed 2-fold ($p = 0.007$) and 5-fold ($p = 0.001$) increase in mononucleotide tract deletions compared to $Mlh1^{+/+}$ jejuna, respectively. Compared to $Mlh1^{-/-}$ jejuna,

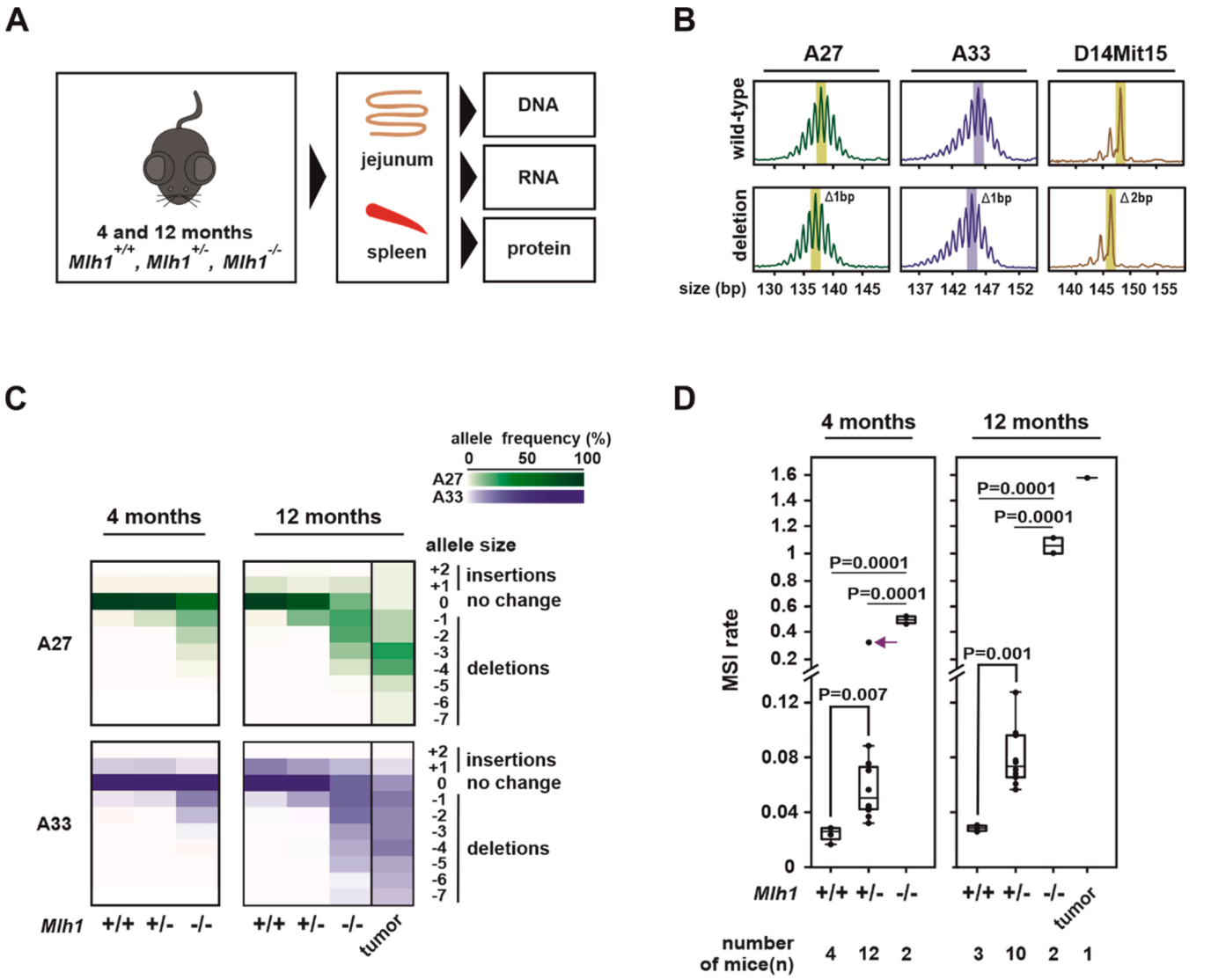

Fig. 1. Normal jejunum of *Mlh1*$^{+/-}$ mice displays MSI at mononucleotide repeats at 4- and 12-month time points. (**A**) Workflow of the study. In mice of the indicated genotypes, we tested *Mlh1* expression (both at mRNA and protein level) and MSI. From DNA samples, we also tested LOH at *Mlh1* gene and assayed *Mlh1* promoter methylation status. (**B**) Representative capillary electropherograms of single-molecule PCR (SM-PCR) based MSI assay for A27, A33 and D14Mit15 microsatellites. Top and bottom panels show electropherograms scored as wildtype and single repeat unit deletion mutant alleles, respectively. The highest peaks (indicated by shading in each electropherogram) were scored; lower peaks are stutter peaks, a typical feature of microsatellite markers. (**C**) Heat map of allele frequency (%) detected at mononucleotide repeats in jejunum of mice of the indicated genotypes, as well as in an intestinal tumor from *Mlh1*$^{-/-}$ mouse. (**D**) MSI rates for deletions in jejunum. Similar data for insertions is shown in **Supplementary Fig. 2.** Statistical testing was performed using unpaired *t*-test. Purple arrow indicates the outlier *Mlh1*$^{+/-}$ mouse. This mouse was excluded from the heat map in (**B**) and is shown separately in **Supplementary Fig. 3**.

on the other hand, they were reduced 9-fold ($p = 0.0001$) and 13-fold ($p = 0.0001$), respectively (Fig. 1**D**). 12-month *Mlh1*$^{+/-}$ jejuna showed a 1.5-fold increase ($p = 0.006$) in deletions compared to 4-month *Mlh1*$^{+/-}$ jejuna (Fig. 1**D**). In contrast to *Mlh1*$^{+/-}$ jejunum, deletion mutant alleles in *Mlh1*$^{-/-}$ jejunum displayed bigger size shifts at both time points, and were more frequent at all three microsatellites (Fig. 1**C–D and Supplementary Fig. 1A–B)**. When comparing deletions at mononucleotide repeats, *Mlh1*$^{-/-}$ jejunum samples had 21-fold ($p = 0.0001$) and 60-fold ($p = 0.0001$) higher deletion rates compared to age-matched *Mlh1*$^{+/+}$ jejuna (Fig. 1**D**). For comparison, the *Mlh1*$^{-/-}$ intestinal tumor showed 90- and 20-fold increase in deletions compared to 12-month *Mlh1*$^{+/+}$ and *Mlh1*$^{+/-}$ jejuna, respectively (Fig. 1**D**).

Unlike what was observed for deletions, at the 4-month time point *Mlh1*$^{+/+}$ jejuna showed an insertional burden at mononucleotide tracts, in particular at A33. Insertions further increased with age in *Mlh1*$^{+/+}$ jejuna (for A33 1.7-fold, $p = 0.01$, and for A27 1.5-fold (p = n.s), see **Supplementary Fig. 2)**. In 4-month-old jejuna, average insertion rates at mononucleotide repeats were similar across all genotypes (*Mlh1*$^{+/+}$, *Mlh1*$^{+/-}$, *Mlh1*$^{-/-}$). However, 4-month *Mlh1*$^{+/-}$ jejuna showed a wide range of inter-individual variation in insertions at A33 (range: 1.7 %–11.9 %). In 12-month-old jejuna, mononucleotide repeat insertions decreased with decreasing *Mlh1* gene dosage (**Supplementary Fig. 2**). Insertions in *Mlh1*$^{+/-}$ and *Mlh1*$^{-/-}$ jejuna were 1.8-fold to 2.9-fold lower when compared to *Mlh1*$^{+/+}$ (**Supplementary Fig. 2**). The decrease in insertions in *Mlh1*$^{-/-}$ jejuna compared *Mlh1*$^{+/-}$ jejuna was not significant (**Supplementary Fig. 2**). Irrespective of genotype or age, insertions in jejunum were almost exclusively single repeat unit in size (1 bp and 2 bp for mono- and dinucleotide repeats, respectively) (Fig. 1**C** and **Supplementary Fig. 1A**).

In general, indels in dinucleotide repeat D14Mit15 were infrequent in *Mlh1*$^{+/+}$ and *Mlh1*$^{+/-}$ jejuna at both time points (**Supplementary Fig. 1**). Mutant alleles at D14Mit15 were predominantly deletions in *Mlh1*$^{+/+}$and *Mlh1*$^{+/-}$ jejuna, and their frequency was similar between the two genotypes. *Mlh1*$^{-/-}$ jejuna showed MSI at D14Mit15 at both

time points (**Supplementary Fig. 1B**). Compared to mononucleotide repeats, deletions at the dinucleotide repeat D14Mit15 were 4.5-fold and 4-fold lower in 4- and 12-month old *Mlh1*$^{-/-}$ jejuna, respectively (Fig. 1**D** and **Supplementary Fig. 1B**).

MSI was also assessed in spleen DNA of the same mice (previously published in [26] and additional new data in **Supplementary Table 1**), enabling comparisons of jejunum MSI to spleen MSI overall, as well as within each mouse. In contrast to *Mlh1*$^{+/-}$ jejuna, there was no substantial increase in mononucleotide repeat deletions in *Mlh1*$^{+/-}$ spleens compared to age-matched *Mlh1*$^{+/+}$, nor did MSI increase with age in either genotype (**Supplementary Table 1**). As in *Mlh1*$^{+/+}$ jejunum, *Mlh1*$^{+/+}$ spleens also showed insertional bias, however, unlike in the jejunum, insertion rates in *Mlh1*$^{+/+}$ and *Mlh1*$^{+/-}$ spleens were comparable (**Supplementary Table 1**). *Mlh1*$^{-/-}$ spleens showed elevated MSI; deletions predominated and increased with age (**Supplementary Table 1**). As in jejunum, the dinucleotide repeat D14Mit15 was stable in *Mlh1*$^{+/+}$ and *Mlh1*$^{+/-}$ spleens at both time points, and *Mlh1*$^{-/-}$ spleens showed elevated MSI (**Supplementary Table 1**).

Inter-individual variation in deletions at mononucleotide repeats was evident in *Mlh1*$^{+/-}$ jejuna in both age groups (Fig. 1**D**). Moreover, one 4-month-old *Mlh1*$^{+/-}$ mouse showed substantially elevated deletions in jejunum (6- and 4-fold higher compared to other age-matched *Mlh1*$^{+/-}$ mice at mononucleotide markers and at D14Mit15, respectively), indicated by an arrow in Fig. 1**D** and **Supplementary Fig. 1B**. With Grubbs' test, this *Mlh1*$^{+/-}$ mouse was classified as an outlier ($p < 0.05$). In this mouse, deletions in jejunum consisted of predominantly

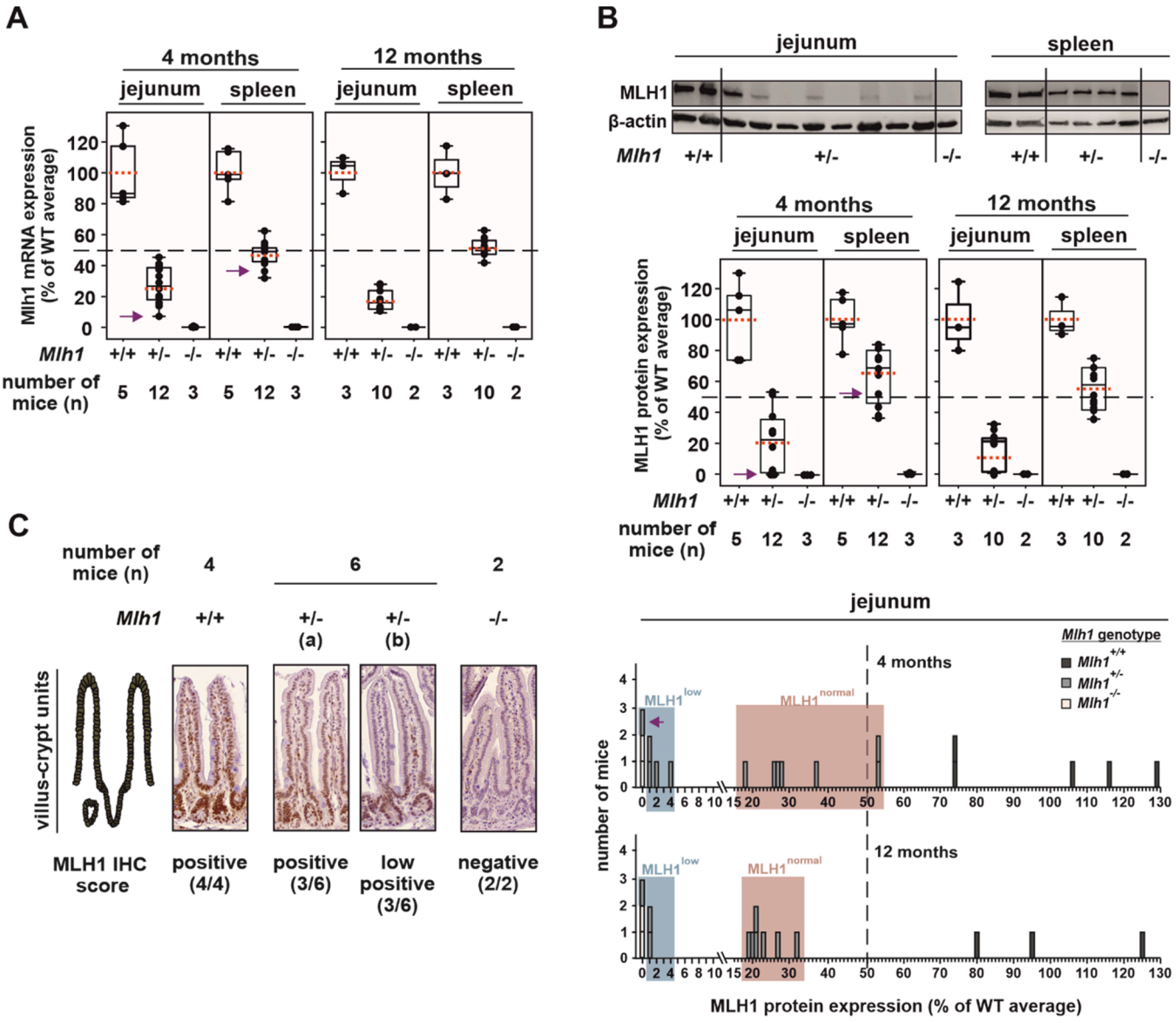

Fig. 2. Jejuna of Mlh1$^{+/-}$ mice show tissue-specific sporadic depletion in MLH1 expression at 4 and 12 months of age. (**A**) Mlh1 mRNA expression analysis. Arrow indicates data point for the outlier Mlh1$^{+/-}$ mouse with high deletion rates at mononucleotide repeats. Red dotted line across each boxplot indicates the average value. Dashed black line across the chart marks 50 % expression level. (**B**) and (**C**) MLH1 protein levels analysis. (**B**) Representative image of western blot. Empty lanes in western blot do not necessarily mean absence of MLH1 but possibly MLH1 protein levels below detectable range of our western blot assay (**Supplementary Fig. 7**). Boxplot shows MLH1 protein expression analysis for the western blots. The red-dotted line across each boxplot represents the average value. The dashed-horizontal line across the chart indicates 50 % MLH1 protein expression. Histogram shows MLH1 protein expression in jejunum of individual mice; genotypes are indicated as black, grey and white. Based on MLH1 protein expression levels, the Mlh1$^{+/-}$ jejuna fall into two distinct sub-groups: one with close-to-expected MLH1 expression (MLH1^{normal}, pink box) and the other with very low MLH1 expression (MLH1^{low}, blue box). Dashed line across the chart marks 50 % MLH1 of wild-type protein expression. (**C**) Representative IHC images of jejunum. Middle two IHC images shows a side-by-side comparison of villus-crypt units scored as (a) positive and (b) low positive by IHC profiler.

one and two repeat shifts (**Supplementary Fig. 3**). We previously reported 4.9 % deletions at mononucleotide repeats in spleen DNA of this mouse (which was 2-fold higher than in other *Mlh1*$^{+/-}$ spleens), while D14Mit15 was stable [26].

3.2. *Mlh1*$^{+/-}$ mice show sporadic decrease in MLH1 expression levels in jejunum

To assess whether the inter-individual variation in deletion frequencies in *Mlh1*$^{+/-}$ jejuna can be explained by *Mlh1* expression levels, we quantified Mlh1 mRNA and MLH1 protein levels using qPCR and western blot, respectively. *Mlh1*$^{+/-}$ spleens, which were microsatellite-stable (**Supplementary table 1**), were used as control tissue. To further examine tissue-specific differences in *Mlh1* expression, we analyzed Mlh1 mRNA expression in brain, kidney and liver using qPCR. We also assessed variation in MLH1 expression by immunohistochemistry (IHC) in jejunum of 4-month-old mice.

In *Mlh1*$^{+/-}$ jejuna, average *Mlh1* expression (both at mRNA and protein levels) was less than the expected ~50 % of *Mlh1*$^{+/+}$ jejuna (Fig. 2**A** and **B**). Further, average expression was lower in the older age group, implying age-dependent MLH1 depletion. In addition, expression levels varied between individual *Mlh1*$^{+/-}$ mice; mice in the 4-month-old group showed more inter-individual variation than those in the 12-month-old group. At 4 months, *Mlh1*$^{+/-}$ jejuna showed on average 26 % Mlh1 mRNA (range: 8 %–46 %) and 21 % (range: 0.4 %–53 %) MLH1 protein expression compared to *Mlh1*$^{+/+}$ levels, and at 12 months the average Mlh1 mRNA and MLH1 protein expression decreased to 16 % (range: 9 %–26 %) and 17 % (range: 0.2 %–32 %), respectively (Fig. 2**A** and **B**). These age-specific decreases in Mlh1 mRNA and MLH1 protein were not statistically significant, however. Based on MLH1 protein expression levels in jejunum, *Mlh1*$^{+/-}$ mice clustered into two sub-groups. One sub-group expressed close-to-expected, that is, approximately 50 % of wildtype MLH1 protein levels (range: 18 %–53 % and 19 %–32 % at the 4- and 12-month time points, respectively), while the other expressed much less MLH1 protein (< 4% at both time points). Henceforth, we refer to these sub-groups of *Mlh1*$^{+/-}$ mice as MLH1^{normal} and MLH1^{low}, respectively (histogram in Fig. 2**B**).

To investigate whether younger mice show similar aberration in *Mlh1* expression levels, we analyzed Mlh1 mRNA expression levels also at 1-month time point. As the older cohorts, 1- month *Mlh1*$^{+/-}$ jejuna also showed less-than-expected- and variable Mlh1 mRNA expression levels (average: 30 %, range: 21 %–37 %) (**Supplementary Fig. 4**). 12-month-old *Mlh1*$^{+/-}$ mice showed a significant decrease in Mlh1 mRNA levels in jejunum ($p = 0.0283$) when compared to 1-month old *Mlh1*$^{+/-}$ mice (**Supplementary Fig. 4**).

Irrespective of age, we observed approximately the expected 50 % Mlh1 mRNA and MLH1 protein levels in all the *Mlh1*$^{+/-}$ spleens (Fig. 2**A,B** and **Supplementary Fig. 4**). Jejunum of the outlier *Mlh1*$^{+/-}$ mouse showed only 8% Mlh1 mRNA expression (Fig. 2A) and no detectable MLH1 protein (Fig. 2**B**), while its spleen had the expected levels of Mlh1 mRNA and MLH1 protein (Fig. 2**A** and **B**).

We also assayed Mlh1 mRNA expression in brain, kidney and liver of two 4-month-old *Mlh1*$^{+/-}$ mice that expressed below age-average Mlh1 mRNA levels in their jejunum; Mlh1 mRNA expression in these tissues were close to the expected ~50 % (60 %, 56 % and 56 %, respectively) (**Supplementary Fig. 5**).

Substantial inter-individual variation in MLH1 protein expression in *Mlh1*$^{+/-}$ jejuna ($n = 6$) was also detectable by IHC. Based on the staining intensity, jejuna of half of the *Mlh1*$^{+/-}$ mice were scored as MLH1-positive and the other half was scored as MLH1 low-positive by IHC profiler (Fig. 2**C**). Upon further analyzing intestinal crypts and villi separately, in MLH1 low-positive jejuna we observed decreased MLH1 staining intensity in both; moreover, all MLH1-negative cells were located in the villi rather than in the crypt (**Supplementary Fig. 6**).

3.3. Tissue-specific depletion of MLH1 in jejunum of *Mlh1*$^{+/-}$ mice associates with constitutive *Mlh1* promoter methylation and not with loss of heterozygosity (LOH) at *Mlh1*

The variable MLH1 protein levels in jejunum of *Mlh1*$^{+/-}$ mice ranging from approximately expected 50 % of *Mlh1*$^{+/+}$ to no expression (Fig. 2**B**) prompted us to investigate possible causes of this sporadic MLH1 depletion. To distinguish between genetic (LOH) and epigenetic (methylation of the *Mlh1* promoter) mechanisms, we performed restriction fragment length polymorphism (RFLP) analysis and methylation-specific PCR (MSP) assay, respectively (Fig. 3**A**).

LOH in *Mlh1*$^{+/-}$ jejuna was tested using RFLP at the 5′ and 3′ ends of *Mlh1* gene (regions spanning exon 1 and exon 19, respectively) (Fig. 3**A**). Out of 22 *Mlh1*$^{+/-}$ jejunum DNA samples assayed ($n = 12$ and 10 for 4- and 12-month time point, respectively), LOH was only observed in the 4-month-old outlier *Mlh1*$^{+/-}$ mouse (Fig. 3**B** and **Supplementary Fig. 8**). Both RFLP_exon 1 and RFLP_exon 19 regions in this mouse had undergone LOH (Fig. 3**B**).

Mlh1 promoter methylation status was assayed using MSP (performed in triplicate, see **Supplementary Fig. 9**). For any given sample, the *Mlh1* promoter was scored as methylated only if PCR products were detected in all MSP triplicates, performed with primers specific to methylated CpG sites. *Mlh1* promoter methylation in jejunum was common (detected in 9/12 and 7/10 *Mlh1*$^{+/-}$ mice at 4 and 12 months, respectively, Fig. 3**C**). Irrespective of age, all *Mlh1*$^{+/-}$ jejuna with very low MLH1 protein expression (<4% of age-matched *Mlh1*$^{+/+}$ jejuna) displayed *Mlh1* promoter methylation (histogram in Fig. 3**C**). Additionally, three 4-month- and four 12-month-old *Mlh1*$^{+/-}$ mice with intermediate MLH1 protein expression (18–28 % of wildtype level) showed *Mlh1* promoter methylation (see Fig. 3**C**, bottom panel). One 4-month-old *Mlh1*$^{+/-}$ mouse with 53 % MLH1 expression showed faint but consistent across-triplicates MSP signal (marked by grey "M" in Fig. 3**C**). Three *Mlh1*$^{+/-}$ mice in each age group did not show *Mlh1* promoter methylation; MLH1 expression in these mice ranged from 21 % to 53 % (Fig. 3**C**).

We then tested *Mlh1* promoter methylation status in additional tissues. For spleen and sperm of six *Mlh1*$^{+/-}$ males each both age groups, *Mlh1* promoter methylation status was reported earlier [26] and here, we expand the cohort by testing *Mlh1* promoter methylation status in spleen of *Mlh1*$^{+/-}$ females ($n = 6$ and $n = 4$ for 4-month and 12-month time point, respectively, **Supplementary Fig. 10**). Irrespective of age, all *Mlh1*$^{+/-}$ mice with *Mlh1* promoter methylation in jejunum also showed *Mlh1* promoter methylation in their spleen, and in the case of males, also in sperm. We further selected three *Mlh1*$^{+/-}$ mice positive for jejunum and spleen *Mlh1* promoter methylation to test for *Mlh1* promoter methylation status in brain, and *Mlh1* promoter methylation was seen there as well (**Supplementary Fig. 10**). None of the *Mlh1*$^{+/+}$ tissues assayed showed *Mlh1* promoter methylation while all *Mlh1*$^{-/-}$ tissues showed *Mlh1* promoter methylation (Fig. 3 and **Supplementary Fig. 10**). Unlike *Mlh1*$^{+/-}$ jejunum, where *Mlh1* promoter methylation status associated with reduced *Mlh1* expression (Fig. 3**C**), all *Mlh1*$^{+/-}$ spleen samples – irrelevant the *Mlh1* promoter methylation status – had the expected, approximately 50 % of wildtype *Mlh1* expression, as quantified both at the RNA and protein level (Fig. 2**A-B**).

3.4. MSI correlates with reduced MLH1 protein level in jejunum of *Mlh1*$^{+/-}$ mice

Within each *Mlh1*$^{+/-}$ jejunum sample, we then explored the relationship between deletion frequency at mononucleotide repeats and MLH1 protein expression. At the 4-month time point, MLH1^{normal} and MLH1^{low} *Mlh1*$^{+/-}$ jejuna displayed 2-fold ($p = 0.002$) and 3-fold ($p = 0.001$) more deletions compared to *Mlh1*$^{+/+}$ (Fig. 4). At the 12-month time point, the increase in MLH1^{normal} and MLH1^{low} *Mlh1*$^{+/-}$ jejuna was 4-fold ($p < 0.0001$) and 7-fold ($P = 0.0009$), respectively (Fig. 4). In jejunum of the *Mlh1*$^{+/-}$ outlier mouse (indicated by arrow in Fig. 4),

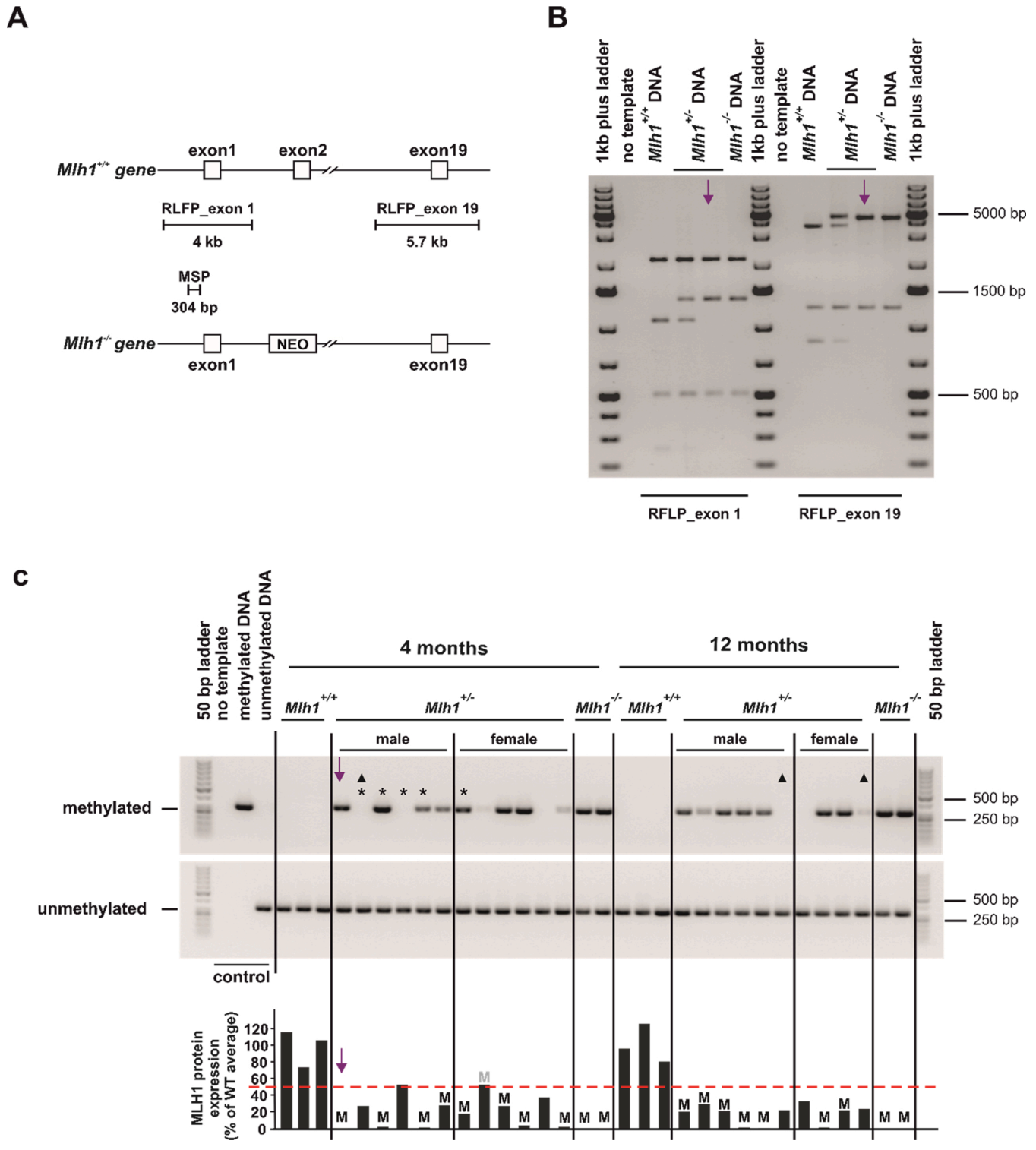

Fig. 3. ***Mlh1*** **promoter methylation, but not** ***Mlh1*** **LOH, is frequent in** $Mlh1^{+/-}$ **jejuna.** (**A**) Schematic of MSP and LOH assay design. MSP and LOH assays were performed in twelve 4-month-old and ten 12-month-old $Mlh1^{+/-}$ mice. (**B**) Representative gel image of PCR-RFLP. Arrow indicates the outlier $Mlh1^{+/-}$ mouse. See **Supplementary Fig. 8** for PCR-RFLP gel images on remaining $Mlh1^{+/-}$ jejunum samples. (**C**) Representative gel image of MSP assay. Histogram below the gel image shows MLH1 protein expression (as % of wildtype average, data from Fig. 2B) for each $Mlh1^{+/-}$ jejunum sample. *Mlh1* promoter methylation per each sample is indicated by "M" (i.e. MSP-positive jejunum samples). "▲" indicates those samples in which MSP signal was detected in only one or two of the MSP triplicates (see **Supplementary Fig. 9)** and were scored as MSP-negative. "M" in grey font indicates faint MSP signal. "*" indicates $Mlh1^{+/-}$ mice for which MSP was also performed in brain. See **Supplementary Fig. 9** for gel images of replicate MSPs for jejuna, ref. [26] and **Supplementary Fig. 10 for** MSP data for spleen, and **Supplementary Fig. 10** for brain. Sample order in **C** is the same as in [26] (males) and as in **Supplementary Fig. 10** (females). Arrow indicates the outlier $Mlh1^{+/-}$ mouse.

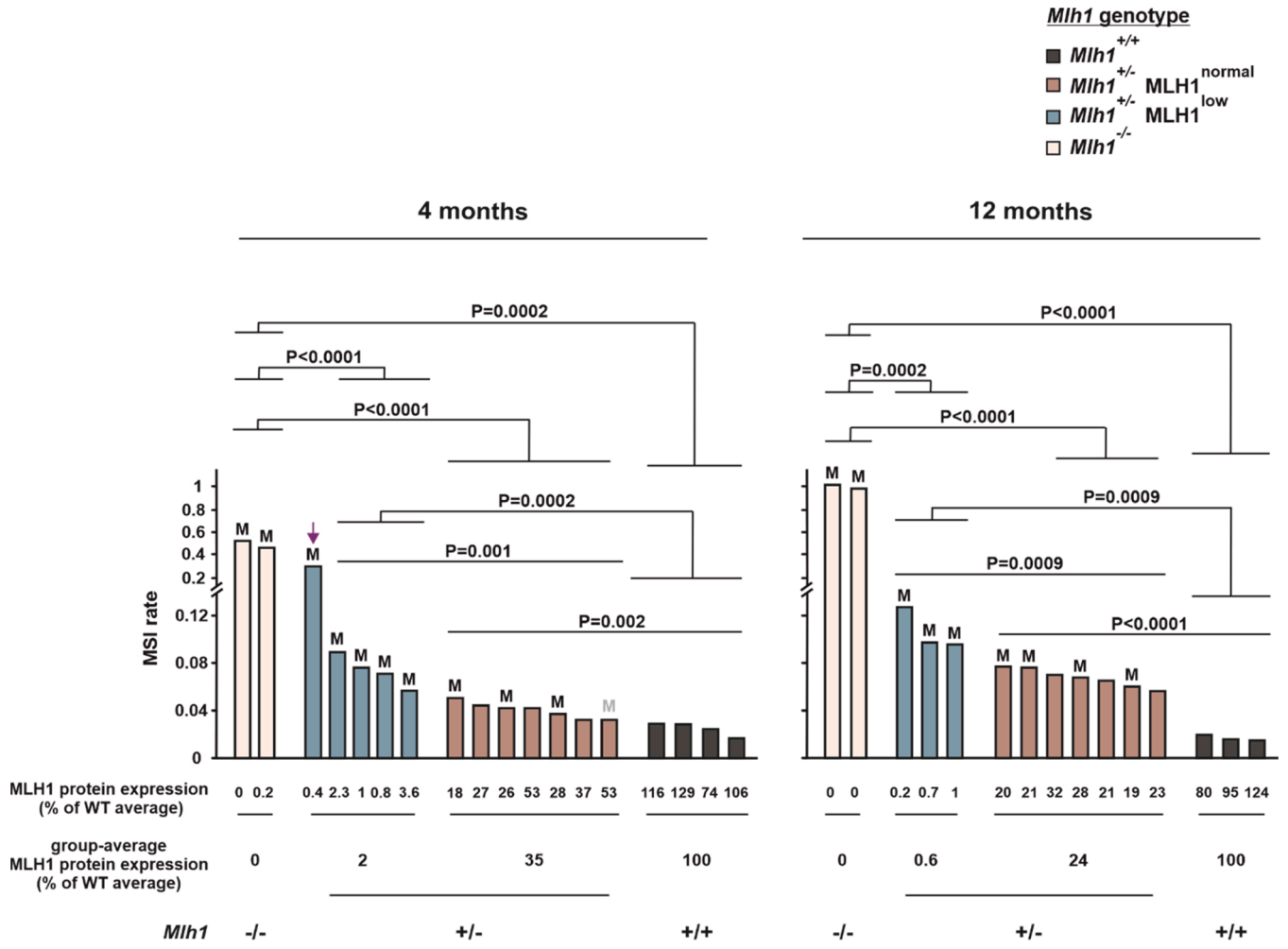

Fig. 4. Deletions at mononucleotide repeats increase with decreasing MLH1 levels in jejunum of *Mlh1*$^{+/-}$ mice. Comparison (unpaired *t*-test) of deletion rates between all genotypes, as well as the two *Mlh1*$^{+/-}$ sub-groups. Arrow indicates the outlier *Mlh1*$^{+/-}$ mouse. "M" indicate those *Mlh1*$^{+/-}$ jejunum samples where *Mlh1* promoter methylation was detected. "M" in grey font indicates faint methylation signal.

there was no detectable MLH1 protein, and deletions were 14-fold more frequent compared to age-matched *Mlh1*$^{+/+}$ jejuna. Linear regression analysis between deletions and jejunum MLH1 expression grouped the two *Mlh1*$^{+/-}$ sub-groups into two distinct clusters, and deletions and MLH1 protein expression showed an inverse correlation at both time points (R^2 = 0.51 and 0.41, and P = 0.0005 and 0.006 for 4- and 12-month time point, respectively) (**Supplementary Fig. 11**). Irrespective of age, all *Mlh1*$^{+/-}$ spleens showed the expected approximately 50 % MLH1 protein level, and no increase in deletions compared to *Mlh1*$^{+/+}$ spleens. The exception was the spleen sample of the outlier *Mlh1*$^{+/-}$ mouse which had 2-fold more deletions compared to age-matched *Mlh1*$^{+/-}$ spleens, despite having normal protein expression level (**Supplementary Fig. 12**).

4. Discussion

Mlh1 mice [7,22] are a powerful model to comprehensively study MSI, and to dissect molecular mechanisms contributing to the MSI phenotype. In line with previous studies [30,36], we observed mononucleotide repeats to be more unstable than dinucleotide repeats. The key to detecting subtle cellular phenotypes with pre-malignant potential, such as low-level MSI, is to employ sufficiently sensitive molecular read-outs. SM-PCR, when applied to unstable microsatellite loci, can detect MSI levels as low as 1%, whereas standard PCR has a detection limit of 20–25 % [37]. Analyzing less unstable microsatellite markers by conventional PCR may result even in failure to detect MSI in *Mlh1*$^{+/-}$ tumors [38].

Overall, MSI in *Mlh1*$^{+/-}$ mice was higher compared to *Mlh1*$^{+/+}$ mice, and increased with age. Further, jejunum-specific MSI varied substantially between *Mlh1*$^{+/-}$ mice of the same age group, and tracked with depleted MLH1 protein levels. These observations are in line with those reported for LS patients who showed inter-individual variation in MSI (including the age at which it was detected) in peripheral blood leukocyte DNA [15]. In addition, already in very young (1-month-old) *Mlh1*$^{+/-}$ mice jejunum-specific inter-individual variation in Mlh1 mRNA levels, and lower-than-expected Mlh1 mRNA levels were observed, suggesting that the cellular changes (including MSI) may occur even earlier.

LS-associated colorectal cancers are MMR-deficient and show high-level MSI, which led to the notion that disruptive mutations in both allelic MMR gene copies are required to instigate the MSI phenotype [9,11]. However, recent evidence of LS-associated adenomas retaining (some) MMR function suggests that the second hit may arise later in the multi-step tumorigenesis than previously appreciated [39], making the idea of pre-tumorigenic MMR haploinsufficiency more plausible. We demonstrate here that MSI is present in normal jejuna of *Mlh1*$^{+/-}$ mice with expected MLH1 levels (approximately 50 % of wildtype), but not in other tissues assayed, indicating tissue-specific MMR haploinsufficiency.

Surprisingly, all *Mlh1*$^{+/-}$ mice harboring *Mlh1* promoter methylation in jejunum also showed *Mlh1* promoter methylation in other tissues

analyzed. *Mlh1* promoter methylation was present in tissues originating from all three germ layers: ectoderm (brain), mesoderm (spleen), endoderm (jejunum), and thus it was likely established already during early embryonic development in these mice. Our study provides first-time evidence of constitutive, but inter-individually stochastic, *Mlh1* promoter methylation in a MMR mouse model. This is analogous to the soma-wide *Mlh1* promoter methylation in suspected LS patients who carry germline MMR epimutations (primarily *Mlh1* promoter methylation) [40–46]. Despite constitutive *Mlh1* promoter methylation in suspected LS patients, malignancies primarily occur in highly proliferating tissues, namely the GI tract, endometrium and skin. Tumors in these patients are MMR-deficient and may or may not show LOH of the unmethylated allele [40]. We show in *Mlh1* mice that despite *Mlh1* promoter methylation in multiple tissues, MLH1 protein depletion is only observed in intestine of these mice; no concomitant LOH was detected. This observation in the pre-neoplastic setting could explain incidence of cancers in suspected LS patients without LOH [40]. Most (72 %) but not all $Mlh1^{+/-}$ mice with constitutive *Mlh1* promoter methylation showed intestine-specific MLH1 depletion, and thus *Mlh1* promoter methylation alone cannot account for the low MLH1 level in *Mlh1* heterozygote jejuna. Likely, other (so far unidentified) underlying regulatory mechanisms impact MMR protein levels in the GI tract. It is worth noting that tissues from $Mlh1^{-/-}$ mice also showed consistent *Mlh1* promoter methylation signal, indicating that the *Mlh1* knock-out allele is also frequently methylated. Obviously, methylation of the promoter of a non-functional gene will not reduce protein level, since the protein is not expressed in the first place. In jejuna of young *Mlh1* heterozygotes, *Mlh1* promoter methylation associated – albeit not perfectly – with MLH1 depletion, while no such clear association was observed in the older cohort. Perhaps in older *Mlh1* heterozygotes, more of the MSP signal originates from the knock-out allele and in such cells, there would be no impact on MLH1 protein levels. In individual cells methylation is not static, but instead a dynamic process where the promoter undergoes de- and re-methylation. We speculate that over time (i.e. in older $Mlh1^{+/-}$ mice), the knock-out *Mlh1* allele may be more likely than the wildtype allele to exist in the methylated state, because de-methylation of a non-functional allele may be less efficient. However, given its strong association with elevated MSI and depleted MLH1 levels in jejunum of young mice, constitutive *Mlh1* promoter methylation has excellent potential as a reporter for early, pre-neoplastic genome instability in tissues vulnerable for MMR-associated tumorigenesis. The fact that *Mlh1* promoter methylation can be scored by MSP on DNA extracted from peripheral blood facilitates its use as a biomarker.

In humans, LS individuals are most susceptible to colorectal and endometrial cancer [40–45]. In $Mlh1^{+/-}$ mice, though overall tumor incidence is low, both GI and non-GI tract tumors, namely lymphoma, cervical squamous cell carcinoma and lung bronchio-alveolar carcinoma, are found [20]. In both humans and mice, tumor spectra associated with defective MMR comprise of proliferative tissues or cell types. Here we show that pre-neoplastic MSI and decreased MLH1 levels specifically impact the intestine, a highly proliferating tissue, in $Mlh1^{+/-}$ mice. Similar, subtle and early molecular events may also prevail in other tissues/cell types with high turnover rate (such as endometrium) making them vulnerable to MMR-dependent tumorigenesis.

Although MSI reports on global MMR defects, MSI *per se* does not necessarily lead to tumorigenesis [20]. If MSI occurs in coding microsatellites, the gene function may be disrupted, which in turn can lead to malignancy and tumorigenesis. Such genes include tumor suppressors and oncogenes which are involved in different regulatory pathways, including cell proliferation, cell cycle, apoptosis, and DNA repair [47, 48]. We did not observe any tumors in $Mlh1^{+/-}$ jejunum, although this observation was limited to mice that were sacrificed to harvest tissues (we did not examine post-mortem the 30 % $Mlh1^{+/-}$ mice which died in our care; **Supplementary Fig. 13**). It is likely that many, if not all, $Mlh1^{+/-}$ mice for which the cause of death was not determined, succumbed to MMR-associated tumors. The 4-month-old outlier $Mlh1^{+/-}$ mouse, whose jejunum had a deletion rate similar to age-matched $Mlh1^{-/-}$ mice, would presumably have had a higher chance of accumulating mutations in MSI-target genes that, over time, may have triggered tumorigenesis in the GI tract of this animal.

This is the first systematic study to establish the relationship between MLH1 levels and MSI in a range of normal murine tissues. MSI in non-neoplastic mucosa [16] and crypt cells [49] has been reported in LS patient samples that likely were MMR-deficient. We demonstrate here that MSI is detectable – albeit at quite a low level – in $Mlh1^{+/-}$ jejunum that still retains close-to-expected (50 % of wildtype) MLH1 protein level, implicating MMR haploinsufficiency in normal, tumor-free $Mlh1^{+/-}$ intestine. High MSI only ensued upon substantial reduction of MMR protein levels. Thus, MMR function appears to rely on a critical threshold level of MMR proteins, in line with *in vitro* studies [17,18]. Importantly, MLH1 depletion was tissue-specific: it was observed only in jejunum and not in other tissues assayed.

Given that the maintenance of genome stability is essential for all cells, it has been puzzling why germline mutations of key DNA repair pathways (mismatch repair, homologous recombination) give rise to cancer only in certain tissues. The tissue-specific haploinsufficiency of *Mlh1* now provides a clue to why the GI tract is vulnerable to MMR-associated cancers. Analogously, heterozygosity of homologous recombination genes, namely *BRCA1* and *PALB2,* also confers subtle genome instability phenotypes that are detectable in pre-malignant cells of mutation carriers, provided that sufficiently sensitive assays are used [50,51]. We propose that tissue-specific decrease in protein levels is an important factor in determining which organs are cancer-prone in heterozygous DNA repair mutation carriers.

CRediT authorship contribution statement

K.S. Shrestha: Conceptualization, Methodology, Software, Formal analysis, Investigation, Resources, Interpretation of data, Visualization, Writing-Original Draft, Writing- Review & Editing. **Liisa Kauppi:** Supervision, Project administration, Funding acquisition, Conceptualization, Methodology, Resources, Interpretation of data, Writing - Review & Editing. **Elli-Mari Aska:** Investigation, Resources, Interpretation of data, Writing - Review & Editing. **Minna M. Tuominen:** Investigation, Resources

Funding

This work was supported by the Academy of Finland grants: 263870, 292789, 256996, and 306026 (to L.K.), Sigrid Jusélius Foundation (to L. K.), and Biomedicum Helsinki foundation grant (to K.S.S).

Declaration of Competing Interest

No conflicts of interest were disclosed.

Acknowledgments

We are grateful to Erika Gucciardo, Manuela Tumiati, Päivi Peltomäki, Marjaana Pussila and Saara Ollila for critical reading of the manuscript, to Elina A Pietilä and Joonas Jukonen for their advice for western blotting experiments, and to members of the Kauppi lab for constructive comments on the figures. We extend our sincere gratitude to the staff of the following core facilities at University of Helsinki: Laboratory Animal Center, Tissue preparation and histochemistry unit, Genome Biology Unit, and FIMM sequencing unit.

Appendix A. Supplementary data

Supplementary material related to this article can be found, in the online version, at doi:https://doi.org/10.1016/j.dnarep.2021.103178.

References

[1] E.R. Fearon, Molecular genetics of colorectal cancer, Annu. Rev. Pathol. 6 (2011) 479–507.
[2] R.W. Burt, Colon cancer screening, Gastroenterology 119 (2000) 837–853.
[3] A. Loukola, R. Salovaara, P. Kristo, A.L. Moisio, H. Kaariainen, H. Ahtola, M. Eskelinen, N. Harkonen, R. Julkunen, E. Kangas, S. Ojala, J. Tulikoura, E. Valkamo, H. Jarvinen, J.P. Mecklin, A. de la Chapelle, L.A. Aaltonen, Microsatellite instability in adenomas as a marker for hereditary nonpolyposis colorectal cancer, Am. J. Pathol. 155 (1999) 1849–1853.
[4] M. Strand, T.A. Prolla, R.M. Liskay, T.D. Petes, Destabilization of tracts of simple repetitive DNA in yeast by mutations affecting DNA mismatch repair, Nature 365 (1993) 274–276.
[5] J. Jiricny, Postreplicative mismatch repair, Cold Spring Harb. Perspect. Biol. 5 (2013), a012633.
[6] L.A. Pray, DNA replication and causes of mutation, Nat. Educ. 1 (2008) 214.
[7] W. Edelmann, P.E. Cohen, M. Kane, K. Lau, B. Morrow, S. Bennett, A. Umar, T. Kunkel, G. Cattoretti, R. Chaganti, J.W. Pollard, R.D. Kolodner, R. Kucherlapati, Meiotic pachytene arrest in MLH1-deficient mice, Cell 85 (1996) 1125–1134.
[8] H. Yamamoto, K. Imai, Microsatellite instability: an update, Arch. Toxicol. 89 (2015) 899–921.
[9] L.A. Aaltonen, P. Peltomaki, F.S. Leach, P. Sistonen, L. Pylkkanen, J.P. Mecklin, H. Jarvinen, S.M. Powell, J. Jen, S.R. Hamilton, et al., Clues to the pathogenesis of familial colorectal cancer, Science 260 (1993) 812–816.
[10] A.G. Knudson Jr., Mutation and cancer: statistical study of retinoblastoma, Proc. Natl. Acad. Sci. U. S. A. 68 (1971) 820–823.
[11] A. Hemminki, P. Peltomaki, J.P. Mecklin, H. Jarvinen, R. Salovaara, M. Nystrom-Lahti, A. de la Chapelle, L.A. Aaltonen, Loss of the wild type MLH1 gene is a feature of hereditary nonpolyposis colorectal cancer, Nat. Genet. 8 (1994) 405–410.
[12] E. Mangold, C. Pagenstecher, W. Friedl, M. Mathiak, R. Buettner, C. Engel, M. Loeffler, E. Holinski-Feder, Y. Muller-Koch, G. Keller, H.K. Schackert, S. Kruger, T. Goecke, G. Moeslein, M. Kloor, J. Gebert, E. Kunstmann, K. Schulmann, J. Ruschoff, P. Propping, Spectrum and frequencies of mutations in MSH2 and MLH1 identified in 1,721 German families suspected of hereditary nonpolyposis colorectal cancer, Int. J. Cancer 116 (2005) 692–702.
[13] P. Peltomaki, Epigenetic mechanisms in the pathogenesis of Lynch syndrome, Clin. Genet. 85 (2014) 403–412.
[14] H. Alazzouzi, E. Domingo, S. Gonzalez, I. Blanco, M. Armengol, E. Espin, A. Plaja, S. Schwartz, G. Capella, S. Schwartz Jr., Low levels of microsatellite instability characterize MLH1 and MSH2 HNPCC carriers before tumor diagnosis, Hum. Mol. Genet. 14 (2005) 235–239.
[15] M.I. Coolbaugh-Murphy, J.P. Xu, L.S. Ramagli, B.C. Ramagli, B.W. Brown, P. M. Lynch, S.R. Hamilton, M.L. Frazier, M.J. Siciliano, Microsatellite instability in the peripheral blood leukocytes of HNPCC patients, Hum. Mutat. 31 (2010) 317–324.
[16] R. Parsons, G.M. Li, M. Longley, P. Modrich, B. Liu, T. Berk, S.R. Hamilton, K. W. Kinzler, B. Vogelstein, Mismatch repair deficiency in phenotypically normal human cells, Science 268 (1995) 738–740.
[17] M. Kansikas, M. Kasela, J. Kantelinen, M. Nystrom, Assessing how reduced expression levels of the mismatch repair genes MLH1, MSH2, and MSH6 affect repair efficiency, Hum. Mutat. 35 (2014) 1123–1127.
[18] M. Kasela, M. Nystrom, M. Kansikas, PMS2 expression decrease causes severe problems in mismatch repair, Hum. Mutat. (2019).
[19] L. Wang, S. Tsutsumi, T. Kawaguchi, K. Nagasaki, K. Tatsuno, S. Yamamoto, F. Sang, K. Sonoda, M. Sugawara, A. Saiura, S. Hirono, H. Yamaue, Y. Miki, M. Isomura, Y. Totoki, G. Nagae, T. Isagawa, H. Ueda, S. Murayama-Hosokawa, T. Shibata, H. Sakamoto, Y. Kanai, A. Kaneda, T. Noda, H. Aburatani, Whole-exome sequencing of human pancreatic cancers and characterization of genomic instability caused by MLH1 haploinsufficiency and complete deficiency, Genome Res. 22 (2012) 208–219.
[20] T.A. Prolla, S.M. Baker, A.C. Harris, J.L. Tsao, X. Yao, C.E. Bronner, B. Zheng, M. Gordon, J. Reneker, N. Arnheim, D. Shibata, A. Bradley, R.M. Liskay, Tumour susceptibility and spontaneous mutation in mice deficient in Mlh1, Pms1 and Pms2 DNA mismatch repair, Nat. Genet. 18 (1998) 276–279.
[21] W. Edelmann, K. Yang, M. Kuraguchi, J. Heyer, M. Lia, B. Kneitz, K. Fan, A. M. Brown, M. Lipkin, R. Kucherlapati, Tumorigenesis in Mlh1 and Mlh1/Apc1638N mutant mice, Cancer Res. 59 (1999) 1301–1307.
[22] S.M. Baker, A.W. Plug, T.A. Prolla, C.E. Bronner, A.C. Harris, X. Yao, D.M. Christie, C. Monell, N. Arnheim, A. Bradley, T. Ashley, R.M. Liskay, Involvement of mouse Mlh1 in DNA mismatch repair and meiotic crossing over, Nat. Genet. 13 (1996) 336–342.
[23] Y. Tokairin, S. Kakinuma, M. Arai, M. Nishimura, M. Okamoto, E. Ito, M. Akashi, Y. Miki, T. Kawano, T. Iwai, Y. Shimada, Accelerated growth of intestinal tumours after radiation exposure in Mlh1-knockout mice: evaluation of the late effect of radiation on a mouse model of HNPCC, Int. J. Exp. Pathol. 87 (2006) 89–99.
[24] M. Herberg, S. Siebert, M. Quaas, T. Thalheim, K. Rother, M. Hussong, J. Altmuller, C. Kerner, J. Galle, M.R. Schweiger, G. Aust, Loss of Msh2 and a single-radiation hit induce common, genome-wide, and persistent epigenetic changes in the intestine, Clin. Epigenetics 11 (2019) 65.
[25] N.J. Toft, D.J. Winton, J. Kelly, L.A. Howard, M. Dekker, H. te Riele, M.J. Arends, A.H. Wyllie, G.P. Margison, A.R. Clarke, Msh2 status modulates both apoptosis and mutation frequency in the murine small intestine, Proc. Natl. Acad. Sci. U. S. A. 96 (1999) 3911–3915.
[26] K.S. Shrestha, M.M. Tuominen, L. Kauppi, Mlh1 heterozygosity and promoter methylation associates with microsatellite instability in mouse sperm, Mutagenesis (2021).
[27] N. Barker, M. van de Wetering, H. Clevers, The intestinal stem cell, Genes Dev. 22 (2008) 1856–1864.
[28] T.L. Crippen, I.M. Jones, Cell proliferation in the bone marrow, thymus and spleen of mice studied by continuous, in vivo bromodeoxycytidine labelling and flow cytometric analysis, Cell Tissue Kinet. 22 (1989) 203–212.
[29] M.A. Beal, A. Rowan-Carroll, C. Campbell, A. Williams, C.M. Somers, F. Marchetti, C.L. Yauk, Single-molecule PCR analysis of an unstable microsatellite for detecting mutations in sperm of mice exposed to chemical mutagens, Mutat. Res. 775 (2015) 26–32.
[30] O. Kabbarah, M.A. Mallon, J.D. Pfeifer, W. Edelmann, R. Kucherlapati, P. J. Goodfellow, A panel of repeat markers for detection of microsatellite instability in murine tumors, Mol. Carcinog. 38 (2003) 155–159.
[31] C.L. Yauk, Y.E. Dubrova, G.R. Grant, A.J. Jeffreys, A novel single molecule analysis of spontaneous and radiation-induced mutation at a mouse tandem repeat locus, Mutat. Res. 500 (2002) 147–156.
[32] A.J. Jeffreys, K. Tamaki, A. MacLeod, D.G. Monckton, D.L. Neil, J.A. Armour, Complex gene conversion events in germline mutation at human minisatellites, Nat. Genet. 6 (1994) 136–145.
[33] G. Covarrubias-Pazaran, L. Diaz-Garcia, B. Schlautman, W. Salazar, J. Zalapa, Fragman: an R package for fragment analysis, BMC Genet. 17 (2016) 62.
[34] C. Moolenbeek, E.J. Ruitenberg, The "Swiss roll": a simple technique for histological studies of the rodent intestine, Lab Anim 15 (1981) 57–59.
[35] F. Varghese, A.B. Bukhari, R. Malhotra, A. De, IHC Profiler: an open source plugin for the quantitative evaluation and automated scoring of immunohistochemistry images of human tissue samples, PLoS One 9 (2014), e96801.
[36] J.W. Bacher, W.M. Abdel Megid, M.G. Kent-First, R.B. Halberg, Use of mononucleotide repeat markers for detection of microsatellite instability in mouse tumors, Mol. Carcinog. 44 (2005) 285–292.
[37] M. Coolbaugh-Murphy, A. Maleki, L. Ramagli, M. Frazier, B. Lichtiger, D. G. Monckton, M.J. Siciliano, B.W. Brown, Estimating mutant microsatellite allele frequencies in somatic cells by small-pool PCR, Genomics 84 (2004) 419–430.
[38] M. Pussila, P. Toronen, E. Einarsdottir, S. Katayama, K. Krjutskov, L. Holm, J. Kere, P. Peltomaki, M.J. Makinen, J. Linden, M. Nystrom, Mlh1 deficiency in normal mouse colon mucosa associates with chromosomally unstable colon cancer, Carcinogenesis 39 (2018) 788–797.
[39] S. Valo, S. Kaur, A. Ristimaki, L. Renkonen-Sinisalo, H. Jarvinen, J.P. Mecklin, M. Nystrom, P. Peltomaki, DNA hypermethylation appears early and shows increased frequency with dysplasia in Lynch syndrome-associated colorectal adenomas and carcinomas, Clin. Epigenetics 7 (2015) 71.
[40] C.M. Suter, D.I. Martin, R.L. Ward, Germline epimutation of MLH1 in individuals with multiple cancers, Nat. Genet. 36 (2004) 497–501.
[41] M.P. Hitchins, J.J. Wong, G. Suthers, C.M. Suter, D.I. Martin, N.J. Hawkins, R. L. Ward, Inheritance of a cancer-associated MLH1 germ-line epimutation, N. Engl. J. Med. 356 (2007) 697–705.
[42] R.C. Niessen, R.M. Hofstra, H. Westers, M.J. Ligtenberg, K. Kooi, P.O. Jager, M. L. de Groote, T. Dijkhuizen, M.J. Olderode-Berends, H. Hollema, J.H. Kleibeuker, R.H. Sijmons, Germline hypermethylation of MLH1 and EPCAM deletions are a frequent cause of Lynch syndrome, Genes Chromosomes Cancer 48 (2009) 737–744.
[43] I. Gazzoli, M. Loda, J. Garber, S. Syngal, R.D. Kolodner, A hereditary nonpolyposis colorectal carcinoma case associated with hypermethylation of the MLH1 gene in normal tissue and loss of heterozygosity of the unmethylated allele in the resulting microsatellite instability-high tumor, Cancer Res. 62 (2002) 3925–3928.
[44] M. Morak, H.K. Schackert, N. Rahner, B. Betz, M. Ebert, C. Walldorf, B. Royer-Pokora, K. Schulmann, M. von Knebel-Doeberitz, W. Dietmaier, G. Keller, B. Kerker, G. Leitner, E. Holinski-Feder, Further evidence for heritability of an epimutation in one of 12 cases with MLH1 promoter methylation in blood cells clinically displaying HNPCC, Eur. J. Hum. Genet. 16 (2008) 804–811.
[45] M.P. Hitchins, The role of epigenetics in Lynch syndrome, Fam. Cancer 12 (2013) 189–205.
[46] A. Goel, T.P. Nguyen, H.C. Leung, T. Nagasaka, J. Rhees, E. Hotchkiss, M. Arnold, P. Banerji, M. Koi, C.T. Kwok, D. Packham, L. Lipton, C.R. Boland, R.L. Ward, M. P. Hitchins, De novo constitutional MLH1 epimutations confer early-onset colorectal cancer in two new sporadic Lynch syndrome cases, with derivation of the epimutation on the paternal allele in one, Int. J. Cancer 128 (2011) 869–878.
[47] A. Duval, R. Hamelin, Mutations at coding repeat sequences in mismatch repair-deficient human cancers: toward a new concept of target genes for instability, Cancer Res. 62 (2002) 2447–2454.
[48] S. Vilkki, V. Launonen, A. Karhu, P. Sistonen, I. Vastrik, L.A. Aaltonen, Screening for microsatellite instability target genes in colorectal cancers, J. Med. Genet. 39 (2002) 785–789.
[49] M. Kloor, C. Huth, A.Y. Voigt, A. Benner, P. Schirmacher, M. von Knebel Doeberitz, H. Blaker, Prevalence of mismatch repair-deficient crypt foci in Lynch syndrome: a pathological study, Lancet Oncol. 13 (2012) 598–606.
[50] S. Pathania, S. Bade, M. Le Guillou, K. Burke, R. Reed, C. Bowman-Colin, Y. Su, D. T. Ting, K. Polyak, A.L. Richardson, J. Feunteun, J.E. Garber, D.M. Livingston, BRCA1 haploinsufficiency for replication stress suppression in primary cells, Nat. Commun. 5 (2014) 5496.
[51] J. Nikkila, A.C. Parplys, K. Pylkas, M. Bose, Y. Huo, K. Borgmann, K. Rapakko, P. Nieminen, B. Xia, H. Pospiech, R. Winqvist, Heterozygous mutations in PALB2 cause DNA replication and damage response defects, Nat. Commun. 4 (2013) 2578.